Chapter 1

Introduction

'How anyone can go out and look up and not want to be an astronomer is beyond me.'

— Richard Preston, *First Light.*

1.1 The Sun

The Sun serves as the primary energy source of the solar system. The dynamic nature of the star gives rise to various physical phenomena like solar storms and auroras on Earth and other planets, making it imperative to understand. The Sun is a typical 4.5 billion-year-old star, classified as spectral type G2 V with an absolute magnitude of 4.8. It has a mass of 1.99×10^{30}kg and a radius of 6.96×10^{8}m. The Sun is located 1.5 million km, or eight light-minutes away, and the emitted radiation amounts to approximately 1366 Wm^{-2} at the top of Earth's atmosphere.

1.1.1 The anatomy of the Sun

The Sun is primarily composed of hydrogen (about 75% by mass) and helium (about 24% by mass) in the photosphere [1, 2]. Other elements—like oxygen (about 1%), carbon (about 0.3%), nitrogen ($\approx$ 0.2%), and oxygen ($\approx$ 0.2%)-make up around 2% of the Sun by mass [3].

Although we cannot directly observe the Sun's interior, theoretical models estimate the core to have a temperature of $\sim 1.5 \times 10^7$ K and a density of about $\sim 1.6 \times 10^5$ kg m^{-3}. These conditions are sufficient for nuclear fusion to occur. The Sun's interior is structured into three main regions: the core, the radiative zone and the convective zone as illustrated in Figure 1.1. The core has half the mass and 1/50 the volume of the entire Sun. But it produces 99% of the energy by nuclear fusion, which slowly moves outward via radiative diffusion to the radiative (or intermediate) zone. In the radiative zone, photons are repeatedly absorbed and re-emitted, slowing their journey toward the solar surface. These interactions cause the wavelength of the photons to increase from high-energy gamma rays in the core to visible light on the solar surface. This is followed by the convection zone, where the energy moves through convective currents and dumps to the solar surface. The movement of the plasma gives rise to magnetic fields originating at the bottom of the convection zone. These magnetic fields propagate upwards, facilitating a continuous exchange of mass and energy between various layers of the solar atmosphere.

The visible solar atmosphere also consists of three distinct layers, each with its unique characteristics. The photosphere – the lowest and densest layer, emits most of the Sun's light and is relatively opaque. Above it is the chromosphere, which is thinner and more transparent, and beyond that lies the corona, which extends outward through a narrow transition region and continues well beyond Earth's orbit. The particle density drops rapidly with altitude—around 10^{23} particles/m^3 in the photosphere to 10^{12} particles /m^3 at a height of one solar radius ($R_\odot$) down to about 10^6 particles/m^3 in the interplanetary medium at one astronomical unit (AU) from the Sun.

An illustration of the temperature variation through the solar atmosphere is depicted on Figure 1.2. Temperature, on the other hand, falls from about 6600 K at the bottom of the photosphere to a minimum value of about 4300 K at the top. Then it rises slowly to about 10000 K in the chromosphere, and then dramatically through the transition region to a million degrees in the corona. The corona expands outwards as solar wind, with the temperature slowly declining to 10^5 K at 1 AU from the Sun [4]. The increase in temperature above the photosphere has been one of the major unresolved problems in solar physics. It is believed that the lower chromosphere is likely heated by sound waves originating from the turbulent convection zone. These waves travel

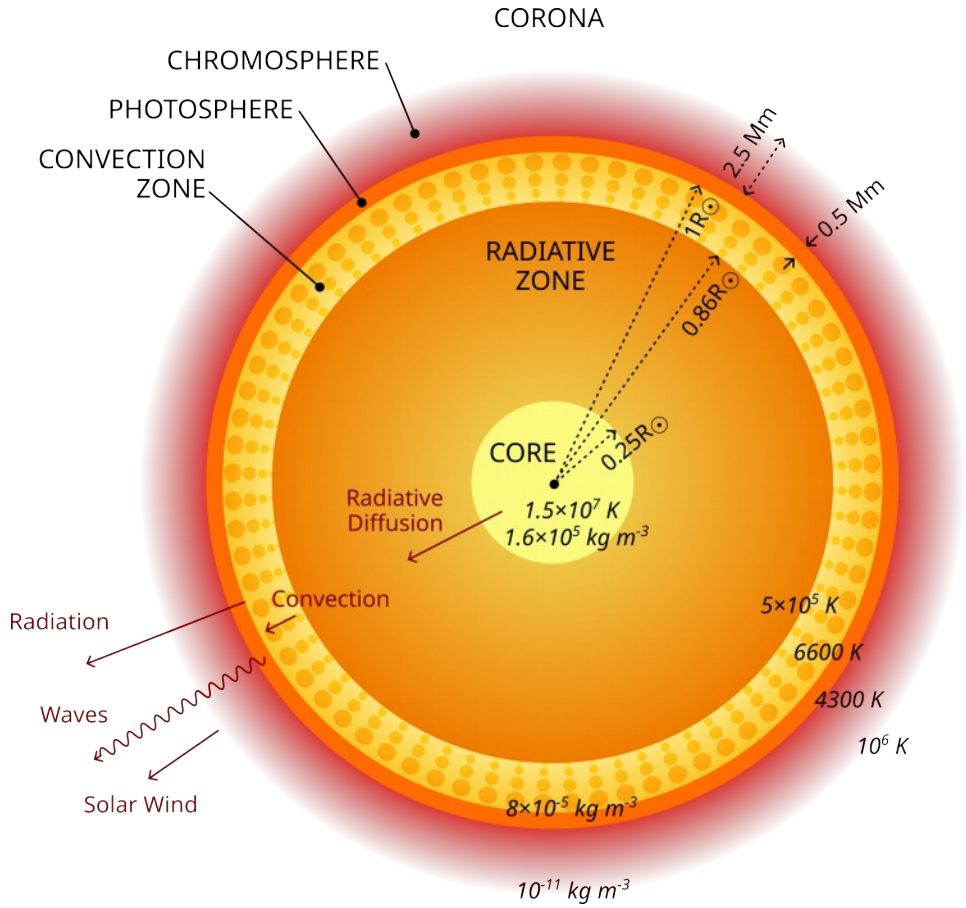

Figure 1.1: An overall structure of the Sun, indicating densities (in kg m^{-3}) and temperature (in K) [4].

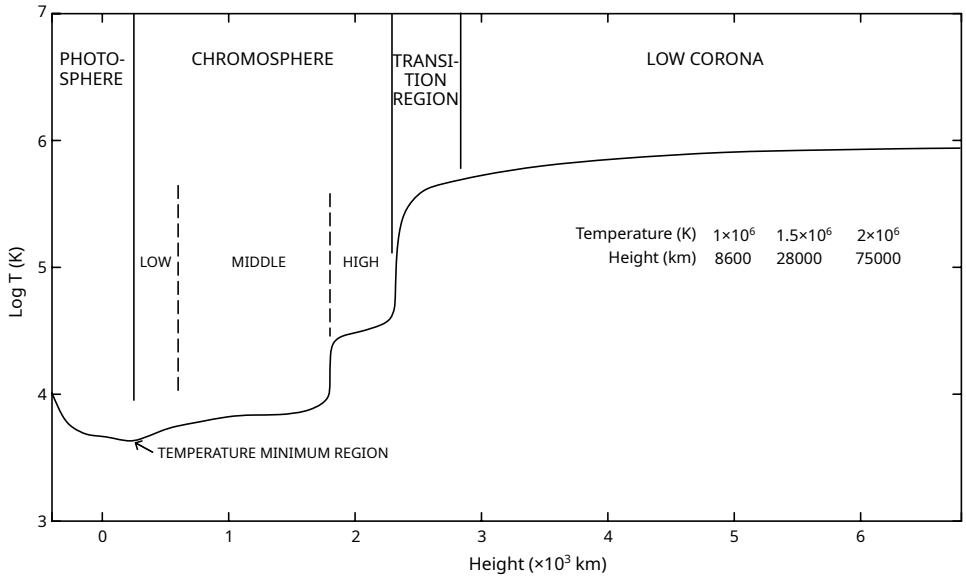

Figure 1.2: The variation of temperature through various heights of the solar atmosphere [4].

outward and release their energy after steepening to form shocks. The upper layers, on the other hand, are likely heated by various magnetic processes.

Majority of the solar illumination comes as a continuous spectrum of light from the solar photosphere, which passes through layers of the Sun's atmosphere. Therefore, the photosphere is best observed in continuum channels in the ultraviolet and visible light. While most of the photospheric light goes straight through, the solar atmosphere absorbs some specific wavelengths due to its increased opacity, making the continuum emission interspersed with characteristic dark absorption lines. These spectral lines provide valuable insights into various solar properties: their intensity reveals temperature, Zeeman splitting indicates magnetic field strength, and Doppler broadening shows the motion of plasma along the line of sight [4]. Most absorption lines occur in the upper photosphere, with some – such as the Balmer lines of hydrogen, Ca II H & K, and Mg II– occurring in the chromosphere. Non-local thermodynamic equilibrium (non-LTE) effects dominate over the radiative transfer in the chromosphere, with most of the light coming from re-emission by these excited species, in contrast to the continuum blackbody emission from the photosphere. Therefore, solar observation in filters of specific wavelengths in the ultraviolet and visible parts of the spectrum can reveal the structure and dynamics of the Sun's atmosphere at various heights.

The chromosphere presents information on the interactions between active-region and network fields with the small-scale magnetic carpet. It can help to better understand the interplay of emerging flux with preexisting fields, wave propagation and mode conversion, mass transport into the corona, and solar wind. The chromosphere also acts as an indicator of coronal activity through thermal conduction or energetic particles, making it essential to understand better.

The transition region (TR) is $\approx$ 100 km high and lies between the cooler chromosphere ($\approx 10^4$ K) and the much hotter corona ($\approx 10^6$ K). Below the TR, the helium is not fully ionized, causing energy to be radiated very effectively. The helium is completely ionized above the TR, which leads to a significant drop in radiation, causing the temperature to rapidly increase through the TR to the corona. The TR emits strongly in UV wavelengths, making it observable with space-based instruments.

The Corona is the outermost layer of the solar atmosphere, first observed during a total solar eclipse. It has a temperature of $\approx 10^6$ K. In the eclipse observations, the corona is visible primarily due to the scattering of photospheric visible light by free electrons. This region is also known as K-corona (*Kontinuierlich* corona). This is dominant within 2.3 solar radii, and its intensity can be directly related to the local electron density. The E-corona (Emission corona), on the other hand, is visible in specific wavelengths due to absorption and remission by ions, and the F-corona (*Fraunhofer* corona), due to photospheric light scattered by interplanetary dust.

1.1.2 Multi-wavelength observations of the Sun

Light from each wavelength band from the Sun reveals unique features associated with different temperatures, heights, and emission mechanisms within the solar atmosphere, ranging from the cooler photosphere to the extremely hot corona. Therefore, observing the Sun at different wavelengths across the electromagnetic spectrum provides a comprehensive understanding of the diverse physical processes occurring in its atmosphere.

Radio and Microwave Observations

At radio and microwave wavelengths, emissions primarily arise from the solar corona and chromosphere. These emissions include both thermal and non-thermal bremsstrahlung, providing valuable insights into the distribution of plasma, magnetic fields, and for a quantitative study of thermal and non-thermal flare emission [5]. Radio observations are particularly useful in studying solar flares, type II and III radio bursts, and coronal mass ejections (CMEs). Some recent observations have also been useful for coronal heating studies.

Infrared Observations

Infrared (IR) observations enable studies of cooler regions of the solar atmosphere originating mainly from the photosphere, chromosphere as well as the

corona. The Ca II (8542 Å) line is particularly of interest to study chromospheric activity, while the He I (10830 Å) is of interest for studying both the corona and chromosphere. In addition, limited studies have been carried out in helioseismology using Mg I (123180 Å) line [6]. However, due to strong atmospheric absorption, IR observations require high-altitude or space-based vantage points.

Visible Light Observations

In the visible light range, most of the observed radiation comes from the photosphere, with certain line emissions coming from the chromosphere. Photospheric features include sunspots, granulation, and faculae. In addition to broadband photospheric observations, spectral lines like the Fe I (6173 Å) line are instrumental in measuring the photospheric magnetic field. Chromospheric features, on the other hand, include prominences around the solar limb, which are popularly seen as colorful structures during a total solar eclipse. Narrowband observations of specific spectral lines, such as Hα (6563 Å) and Ca II H & K (3968 Å and 3933 Å, respectively), help image the chromosphere and study chromospheric dynamics.

Ultraviolet Observations

Ultraviolet (UV) and extreme ultraviolet (EUV) wavelengths are emitted by the hotter, upper layers of the solar atmosphere, including the chromosphere, transition region, and corona. The Earth's atmosphere attenuates solar radiation in these bands, making it essential for observations from space. Instruments such as the Atmospheric Imaging Assembly on Solar Dynamics Observatory's (SDO/AIA) [7] and the Transition Region and Coronal Explorer on Solar and Heliospheric Observatory (TRACE/SOHO) [8] have been pivotal in observing features such as coronal loops, solar flares, and active regions in the UV and EUV bands (Lemen et al., 2012; Domingo et al., 1995). However, there have been limited spatially resolved observations in the near-ultraviolet regime, which is discussed in section 1.2

X-ray Observations

X-rays originate from extremely hot coronal regions and are predominantly associated with solar flares and active regions. Processes like magnetic reconnection produce these high-energy emissions. Spatially resolved X-ray observations from instruments like RHESSI [9] and Hinode/XRT [10], and continuous disk-integrated monitoring with the GOES X-ray detectors have provided crucial data on the temporal and spatial evolution of solar flares and coronal heating mechanisms.

1.2 The need for near-ultraviolet solar observations and the challenges therein

The NUV wavelengths mainly originate from the solar photosphere and chromosphere, thereby helping us understand the dynamic coupling between these magnetized layers. High-resolution NUV imaging enables a detailed study of NUV irradiance from solar flares, which might hold key indications of early flare signatures [11]. Moreover, combining flare observations from these images with those recorded in EUV and X-rays will help us develop a complete spectral energy distribution of solar flares. This is crucial to understanding the energetics in these dynamic events.

Additionally, NUV studies of the Sun is instrumental in studying the atmospheric chemistry of the Earth, as it absorbs high-energy solar radiation, particularly in the X-ray and ultraviolet (UV) spectra. Solar UV radiation below 200 nm is primarily absorbed by oxygen (O_2). Within the range of 200 nm to 242 nm (Herzberg continuum), both oxygen (O_2) and ozone (O_3) contribute to absorption, with ozone playing a more significant role above 242 nm (Hartley Band). UV radiation beyond 310 nm (Huggins Band) generally penetrates the Earth's atmosphere. Consequently, solar radiation within the 200 nm to 400 nm wavelength band plays a crucial role in shaping the atmospheric chemistry and climatic dynamics of our planet. Also, more than 60% variability over a solar cycle is recorded in radiation below 400 nm [12]. However, radiation with a shorter wavelength than 400 nm accounts for just 8% of total solar irradiance (TSI). These broad bands of light play a central role in

understanding the effects of solar radiation on the dynamics and chemistry of the terrestrial atmoshere, and the climate dynamics on the Earth. It is to be noted that the variability in TSI over a solar cycle is $\approx 0.1\%$. Sun-as-a-star measurements by the SIM instrument on SORCE suggested irradiance changes between 2007 and 2004 to be greater by 3 – 6 times than that predicted by state-of-the-art models [13]. However, this data does not help identify any solar features that might be causing the irradiance changes, which can be solved by spatially resolved imaging of the solar atmosphere in the NUV band.

Historically, the Calcium H & K lines at 396.85 nm and 393.4 nm have been instrumental in chromospheric observations. However, Magnesium is approximately 18 times more abundant than calcium in the solar atmosphere [14]. Mg II h&k lines form at a higher level in the solar atmosphere compared to the analogous Ca II H&K lines. The Mg II h&k resonance doublets at 280.3 nm and 279.6 nm are among the strongest solar spectral lines, making them very valuable for studying chromospheric diagnostics [15]. Limited observations indicate that magnesium resonance lines probe a different region of the solar atmosphere compared to the Calcium lines. The calcium H&K lines often lack emission reversals or display single-peaked profiles [16]. However, the magnesium lines consistently exhibit double-peaked emission reversals, except in sunspots [17]. Additionally, the strong red-blue asymmetry observed in the Ca II H&K lines, which are believed to result from acoustic waves steepening into shocks [18], is significantly less prominent in the Mg II h&k lines [19]. This makes these Magnesium lines significant indicators of chromospheric activity.

One of the major limitations of ground-based NUV observations is heavy atmospheric attenuation of these wavelengths by the ozone layer. On the other hand, the solar irradiance increases by two orders of magnitude in this wavelength range as depicted in Figure 1.3. The figure shows the concatenated spectra from sun-as-a-star observations by SOLar STellar Irradiance Comparison Experiment (SOLSTICE; 115–320 nm) onboard the SOlar Radiation and Climate Experiment (SORCE) [20–22] satellite and SOLar SPECtrometer (SOLSPEC; $>$ 320 nm) [23]. This makes space-based observations in this NUV band very challenging, even from space, as it is tough to accommodate the entire band within the dynamic range of one instrument. The limited scope of solar observation in the NUV band leaves a major gap in observing the solar chromosphere and understanding Sun-Earth climatic interactions.

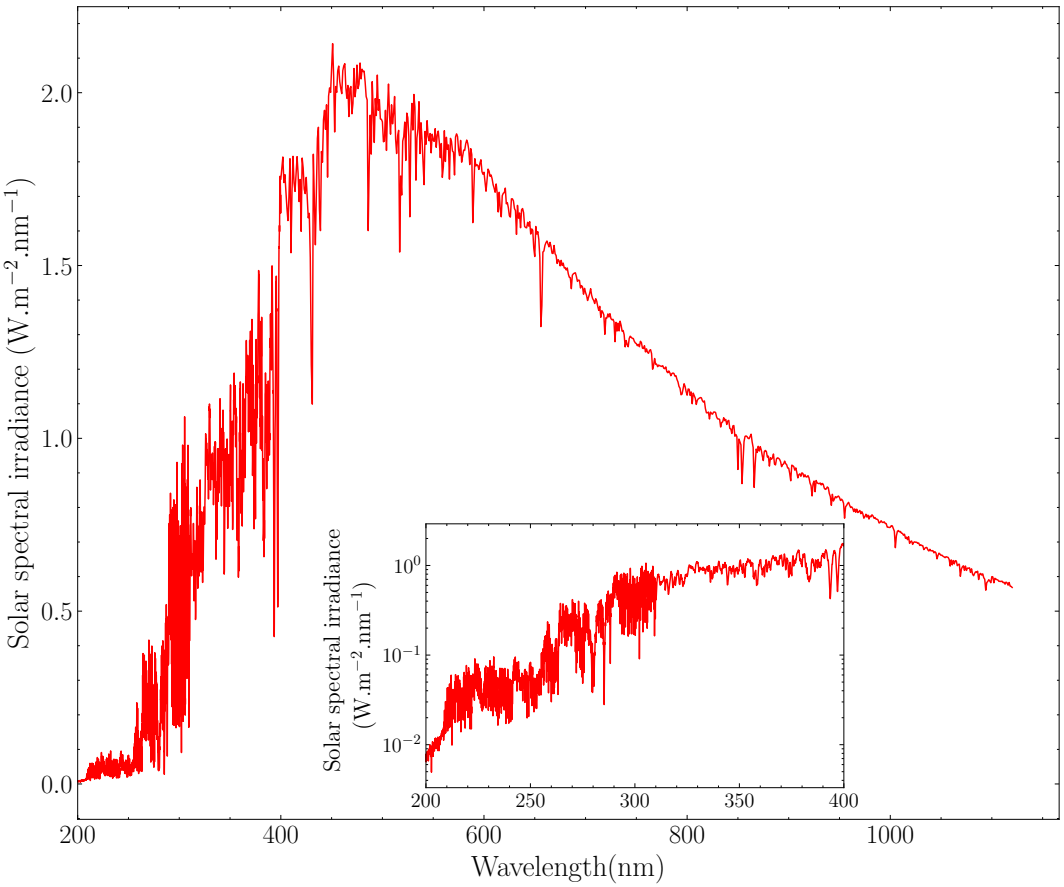

Figure 1.3: The solar spectrum from SOLSTICE and SOLSPEC combined. The inset plot shows approximately two orders of magnitude rise in solar irradiance within *SUIT*'s observation band.

1.3 Solar Observations in NUV

There have not been any full-disk spatially resolved observations in the 200-400 nm band, except in Ca II H&K. The Ultraviolet Spectrometer and Polarimeter (UVSP) [24] on the Solar Maximum Mission (SMM) [25], and the Interface Region Imaging Spectrograph (IRIS) [26] have had limited spatial and spectral coverage in these wavelengths. IRIS records full disk mosaics of the Sun, which cannot give simultaneous imaging of the entire solar disk. Additionally, in terms of photometry, the absolute throughput of IRIS is derived from the efficiency curves of each individual optical element. Post-launch, this is done by observing B-type stars or by comparing the full-disk mosaic measurements with co-temporal sun-as-a-star SORCE/SOLSTICE or TIMED/SEE observations [27].

Two flights of the balloon-borne *Sunrise* mission also covered this complete wavelength range. The *Sunrise Filter Imager (SuFI)* facilitates observation at 214 nm with 10 nm bandwidth, 300 nm with 5 nm bandwidth, 388 nm with 0.8 nm bandwidth, and 396.8 nm (core of Ca II h) with 0.18 nm bandwidth [28], which are similar to some of the observation bands of *SUIT* as mentioned in Table 1.2. However, the observations from *Sunrise* were for a short period of time, with very small field of view and extremely high resolution [28, 29] ($\approx$ 0.02 arcsec/pixel). On-ground contrast transfer, spatial resolution tests, and distortion tests were performed for this instrument [30]. However, SuFI did not undergo any on-ground or on-board photometric calibration. The instrument measured relative contrast values at extremely small spatial scales, but not in the absolute photon fluxes. The *Sunrise Ultraviolet Spectrograph and Imager (SUSI)* [31] instrument also covered 309 nm in the third flight of Sunrise but at extremely high resolution and with small field of view.

To tackle these challenges, the Solar Ultraviolet Imaging Telescope [*SUIT*; 32–34] has been designed for high-cadence, spatially resolved observations of the entire solar disk in the 200 – 400 nm wavelength range from space. Launched on September 2, 2023, it is an instrument on board Aditya–L1 mission of the Indian Space Research Organization (*ISRO*) [35, 36], which is currently placed in a halo orbit around the Sun-Earth Lagrange 1 point,

facilitating uninterrupted 24×7 solar observation.

1.4 The Solar Ultraviolet Imaging Telescope

The Solar Ultraviolet Imaging Telescope (*SUIT*) is an off-axis Ritchey-Chrétien type telescope with a focal length of 3500 mm at f/24.8, facilitated by off-axis hyperbolic primary and secondary mirrors. Imaging is performed on a back-thinned, back-illuminated, UV-enhanced CCD. The CCD is a square array of 4096 × 4096 pixels, each 12 μm size. This gives *SUIT* a plate scale of 0.7″/pixel and a field of view of $0.8^\circ \times 0.8^\circ$, corresponding to 1.5 $R_\odot$ [37]. The instrument is designed to deliver a spatial resolution of 1.4″making it capable of resolving structures of the order 10^3 km on the solar surface.

To accommodate the two-order-of-magnitude increase in solar flux in the 200 - 400 nm wavelength range within *SUIT* dynamic range and get sufficient SNR in the observations, it uses a specific combination of filters with each bandpass filter. *SUIT* has 8 narrowband (NB) filters, 3 broadband (BB) filters, and 5 combination filters mounted on two filter wheels, each having eight slots. A given filter combination is achieved by rotating the two filter wheels independently and placing the desired filter combination in the beam path [33, 34]. Figure 1.5 shows the schematic diagram and a photograph of *SUIT*. Table 1.1 shows the specifications of the instrument.

With its capabilities, *SUIT* broadly seeks to achieve the following science goals-

- **Coupling and dynamics of the solar atmosphere:** What are the processes through which the energy is channelized and transferred from the photosphere to the chromosphere and then to the corona?
- **Prominence studies from *SUIT*:** What are the mechanisms responsible for stability, dynamics and eruption of solar prominences?
- **Solar flare studies:** What is the effect of solar flares on the chromosphere? At what wavelength do solar flares carry maximum energy? What is a solar flare like in its early stages and how does it influence the early phase kinematics of coronal mass ejections?

Parameter	Value
Telescope	
Design	f/24.8 two mirror off-axis design
Entrance Aperture	146 mm
Primary mirror diameter	140.8 mm
Focal Length	3500 mm
Detector	
Type	4096 × 4096, back-thinned, back-illuminated, UV-enhanced CCD
Full-well capacity	195,000 e^-
Plate Scale	0.7 arcsecond/pixel @ 12 μm pixel
Field of View (FOV)	2860× 2860 arcsecond^2
Cadence	
Full Frame	20 s
Region of Interest (RoI)	4 s
Filters	
Entrance aperture	blocking (out band)
Science filters	8 Narrow-band, 3 Broad-band
Exposure times	0.1 to 1.4 s
Mass	42 Kg
Power	35 W
Daily Data Volume	42 GB, uncompressed
Compression	Factor of 2, Lossless

Table 1.1:: Technical specifications of the Solar Ultraviolet Imaging Telescope (*SUIT*)

- **Sun-climate studies with *SUIT*:** What is the effect of UV irradiance variation on the chemistry of Earth's upper atmosphere? How do the Sun-Earth connections concern Earth's climate?

1.4.1 Subsystems of *SUIT*

SUIT comprises three primary subunits, the telescope assembly, payload electronics (PE), and the filter wheel drive electronics (FWE). We shall refer to the telescope assembly when we mention *SUIT* throughout the entire text. The telescope assembly is mounted on the top deck of Aditya-L1, next to the Visible Emission-Line Coronagraph instrument, as illustrated in Figure 1.4. The PE and FWE are mounted in the intermediate deck of the spacecraft. These packages will be addressed explicitly wherever necessary. The PE package consists of the driver electronics for all electronic components of the telescope assembly. The PE box executes the operational modes, including the onboard intelligence for flare detection, localization, and tracking, and provides interfaces with spacecraft subsystems and other instruments. The FWE operates the two filter wheels based on the sequence supplied by the PE box.

The *SUIT* telescope assembly comprises of the following sub-units:

- **Thermal Filter Assembly:** The thermal filter assembly (TFA) forms the entrance aperture of the instrument. This optical component allows 0.1% of the incoming sunlight from entering the payload cavity, to maintain a reasonable temperature of $\approx 20^{\circ}$C inside the telescope enclosure. It also reduces the incoming solar flux within the operational wavelength between 200–400 nm to ensure CCD linearity and desired photometric performance. Figure 3.11 shows a schematic diagram and photograph of the TFA.

- **Primary and Secondary Mirror Assemblies:** The primary and secondary mirrors are off-axis concave and convex hyperbolas having diameters of 141 mm and 49 mm, respectively. They are fabricated on Zerodur substrates and provide $> 86\%$ reflectance in the 200-400 nm band. Figure 3.2 shows the flight model of the mirror assemblies.

- **LED Array:** The *SUIT* LED unit is necessary to illuminate the CCD,

to check pixel-to-pixel variation of response. The calibration unit has 16 LEDs, with 8 LEDs having peak transmission at 258 nm, and the other 8 at 356 nm. LEDs of one wavelength are grouped in sets of 4 main and 4 redundant. Operating one set of 4 creates an even illumination on the CCD. The light from the LEDs pass through the science and complementary filters and the field corrector lens before reaching the CCD.

- **Filter wheel assembly:** The filter wheel assembly of *SUIT* holds 11 science filters and 5 complementary filters. The science filters select the scientific band of interest, while the complementary filters ensure sufficient SNR to perform imaging. Each filter wheel has 8 slots and can be rotated independently to select the desired combination of filters. CAD model and a photograph of the filter wheel assembly are shown in Chapter 2. Table 1.2 shows the filter combinations used in *SUIT*. Further details on the science filter assembly can be found in Chapter 2.

- **Field Corrector Lens Assembly:** The Field Corrector Lens Assembly (FCLA) is a positive meniscus lens mounted on a piezo linear stage allowing ± 3mm of motion. This unit improves the system's optical performance, especially at high field angles. A photograph of this unit is shown in Figure 3.4.

- **Detector Housing Assembly (DHA):** The Detector Housing Assembly (DHA) is the final component in the optical path of *SUIT*. The detector is a Charge-Coupled-Device (CCD) manufactured by Teledyne e2v (UK) Ltd. The CCD is a square array of 4096×4096 pixels, with a pixel size of $12\mu m$ and four readout amplifiers. The CCD is mounted to the optical bench with a detector housing assembly (DHA). This provides proper mounting of the detector, along with the necessary mechanical support and thermal interfaces. The detector is cooled to -55°C giving dark current of 4 e pix^{-1} s^{-1}. The cooling is achieved with a radiator plate and an ethane heat pipe, which conducts heat from the CCD to the radiator, acting as a cold finger. Figure 3.10 shows the CAD model and a photograph of the flight model of the DHA.

Each optical component and sub-unit was optically tested and then qual-

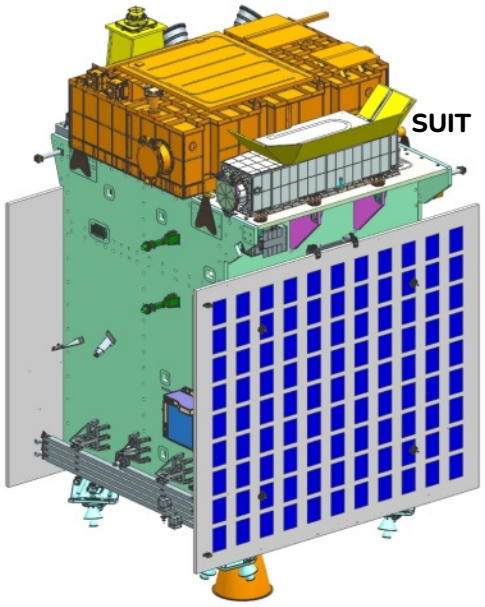

Figure 1.4: A CAD model of the Aditya-L1, illustrating the position of *SUIT* on the spacecraft [34].

Science Filter	Comb. Filter	Central Wavelength (nm)	Bandpass (nm)	Science target
NB01	BB01	214.0	11.0	Continuum
NB02	BP02	276.6	0.4	Mg II k blue wing
NB03	BP02	279.6	0.4	Mg II k
NB04	BP02	280.3	0.4	Mg II h
NB05	BP02	283.2	0.4	Mg II h red wing
NB06	BP03	300.0	1.0	Continuum
NB07	BP03	388.0	1.0	CN Band
NB08	NB08	396.85	0.1	Ca II h
BB01	BB01	220.0	40.0	Herzberg Continuum
BB02	BP04	277.0	58.0	Hartley Band
BB03	BP04	340.0	40.0	Huggins Band

Table 1.2:: List of *SUIT* bandpasses and the facilitating filters with the corresponding central wavelengths, transmission bandwidth (Full Width at Half of Maximum for Narrowband (NB) filters and 99% transmission bandwidth for Broadband (BB) and Bandpass (BP) filters), and the observation interest [38].

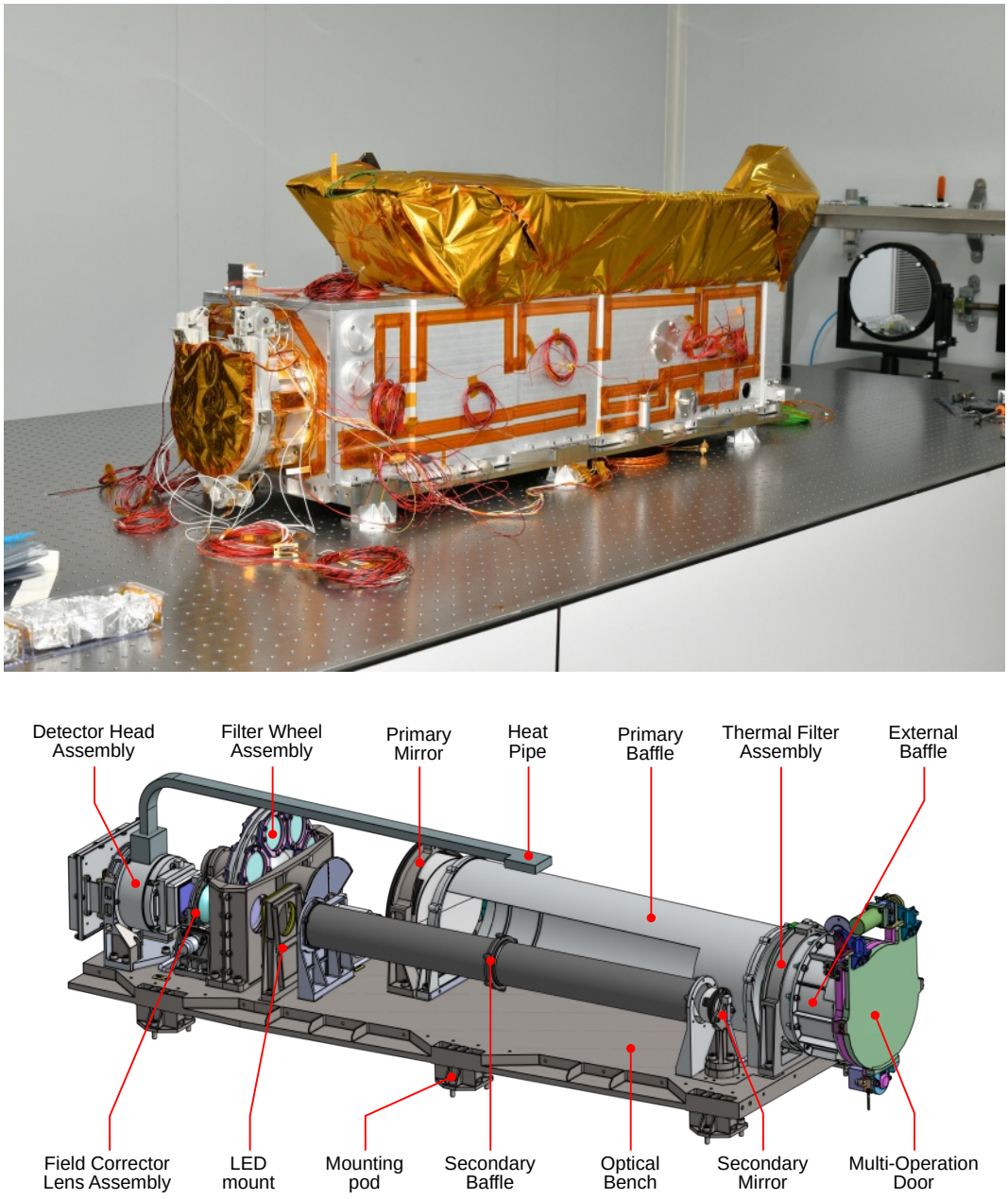

Figure 1.5: A schematic diagram [top] and a photograph [bottom] of the *SUIT* payload.

ified for spaceflight. The components were then mounted on an optical bench and aligned with high accuracy to get high-quality images from *SUIT*. Figure 1.6 displays fully calibrated science-ready full disk images recorded on May 17, 2024, in all eleven filters of *SUIT*.

1.5 Motivation and Outline of the Thesis

This thesis presents a detailed description of the development of *SUIT*, starting from the optical alignment of the instrument, to the in-lab testing of the payload and its subsystems. This is followed by a detailed description of the on-board test and calibration of *SUIT* to ensure it delivers high-quality science-ready NUV data of the Sun.

Being motivated by the presented aspects, the following objectives have been set to address in this research:

- Space-environment qualification, optical testing and characterization of *SUIT* science filters.
- Optical alignment and mechanical integration of the *SUIT* payload.
- Photometric calibration and spectral validation of *SUIT*.
- Pre- and post-flight test and calibration of *SUIT*.

Chapter 1 explains the gap in solar observation that *SUIT* covers. The chapter starts by presenting the various layers of the solar interior and atmosphere. It puts forward the importance of spatially resolved near ultraviolet solar observations. There have been limited observations in this band, from both ground and space, which were also limited in spatial and spectral coverage. This justifies the need to fill the gap of full disk NUV solar observations with high cadence, which is met by *SUIT*. The chapter gives a brief overview of *SUIT*, followed by a detailed explanation of every significant component and sub-assembly.

The *SUIT* payload features 11 science bandpasses designed to observe different layers of the solar atmosphere and study solar irradiance's impact

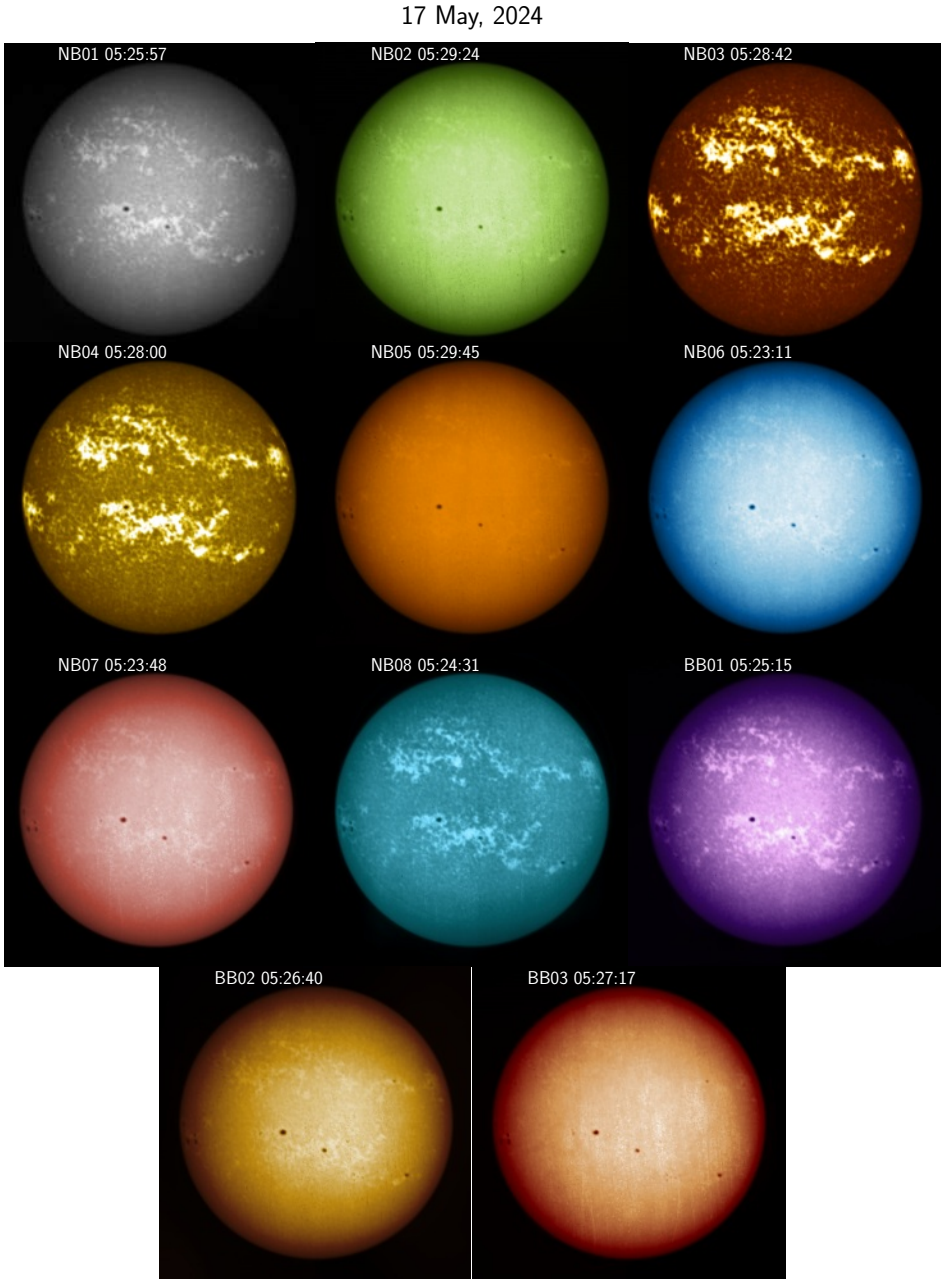

Figure 1.6: Full disk images in all eleven filters recorded by SUIT on May 17, 2024.

on Earth's climate. It utilizes eight narrowband (NB) and three broadband (BB) filters with five complementary filters. Chapter 2 presents a detailed account of the characterization of these science filters. The bandpasses of these filters are very sensitive to changes in operational conditions. The change in transmission with temperature, humidity, and proton irradiation are tested to validate the filters' resilience to space conditions. Performance characterization involved analyzing spatial transmission variation, tilt-dependent transmission shifts, and out-of-band transmission. The correct tilt angles are identified, and the filters are mounted to the filter wheels, ensuring appropriate bandpass and stringent contamination control.

The *SUIT* payload has multiple optical sub-units, *viz.*, the thermal filter, primary and secondary mirrors, field corrector lens assembly, science filters and the CCD. These components have to be aligned meticulously to ensure good image quality. Chapter 3 explains the optical alignment procedure of *SUIT*, along with the optical metrology methods and techniques used to verify the reproduced image quality. The details of full payload integration, such as the routing of electronic cables and mounting of all non-optical sub-units, such as cover panels, baffles, etc., are presented. The mounting of *SUIT* on the Aditya-L1 satellite deck and methods used for co-alignment of *SUIT* with the satellite coordinate system are also explained in detail, along with the final alignment results.

Chapter 4 presents the photometric calibration and spectral validation of the *SUIT* payload performed after payload qualification tests. *SUIT* is the first full-disk solar telescope operating in the 200–400 nm wavelength band, except the Ca II H&K lines. Therefore, a complete photometric calibration is of utmost importance for irradiance measurement of various solar features. Spectral validation is necessary to check the end-to-end response of *SUIT* across wavelengths of a bandpass. An elaborate calibration setup is developed with the payload in an ultra-clean high vacuum environment, with a collimator directing monochromatic light into it. The flight spare model of *SUIT* is used as the collimator due to its high UV reflectance and good optical quality. These measured values are compared with the forward-modeled throughput derived from Sun-as-a-star spectrum using SOLar STellar Irradiance Comparison Experiment (SOLSTICE) onboard the SOlar Radiation and Climate Experiment (SORCE) [20–22] satellite and SOLar SPECtrometer (SOLSPEC) [23]. The

results confirm that the spectral response of *SUIT* aligns with its designed observation bands. Additionally, lab-measured throughput closely matches the modeled throughput, validating the optical performance of *SUIT* and ensuring the reliability of its developed calibration model.

Chapter 5 presents the methodology for the pre-flight and post-flight test and calibration of *SUIT*. Raw, Level 0 *SUIT* data is calibrated using several modules running on the *SUIT* image processing pipeline to prepare science-ready Level 1 data products. This is done using several calibration frames, which were recorded on the ground, as well as in space. These corrections include dark, bias, and flat field corrections, normalizing the pixel response non-uniformity, and removing scattered light and ghost reflections. In this chapter, we explain the procedure of creating the calibration frames and the calibration process. We also present the level of correction implemented on the images. Several parameters defining the pre- and post-flight optical properties of *SUIT* are evaluated. These include the point spread function (PSF), modulation transfer function (MTF), plate scale, and field of view (FOV). All the tested parameters are seen to comply with the design values except for the spatial resolution.

The thesis concludes in Chapter 6 with an overall account of the work accomplished, and the ground and space-based test results summarized.